Supplementary information:
Optimized instrument configurations for tandem particle mass analyzer and single particle-soot photometer experiments

A. Naseri[1], T. A. Sipkens[1,2], S. N. Rogak[2], J. S. Olfert[1] *

[1] *Department of Mechanical Engineering, University of Alberta, Edmonton, Canada.*
[2] *Department of Mechanical Engineering, University of British Columbia, Vancouver, Canada*

* To whom the correspondences should be addressed:
Email: jolfert@ualberta.ca
Office Tel: 780-492-2341

1 Computing m_p-m_{rBC} phantom distributions

1.1 Mathematical form

In the present work, phantom m_p-m_{rBC} distributions are taken as joint lognormal. Distributions are phrased in terms of $\log_{10}$-space, that is $\partial N/(\partial \log_{10} m_p \cdot \partial \log_{10} m_{rBC})$ rather than $\partial N/(\partial m_p \cdot \partial m_{rBC})$, as the particle mass spans several orders of magnitude. Distributions are parameterized following Sipkens et al. (2020b), phrasing the distributions as bivariate normal in $\log_{10}$-space, using Eq.8 of the paper. In that equation, the mean is,

$$\boldsymbol{\mu} = [\log_{10} m_{\mathrm{rBC,g}}, \log_{10} m_{\mathrm{p,g}}]^{\mathrm{T}}, \tag{S1}$$

and the covariance is,

$$\boldsymbol{\Sigma} = \begin{bmatrix} (\log_{10}\sigma_{\mathrm{rBC}})^2 & R_{12}\log_{10}\sigma_{\mathrm{p}}\log_{10}\sigma_{\mathrm{rBC}} \\ R_{12}\log_{10}\sigma_{\mathrm{p}}\log_{10}\sigma_{\mathrm{rBC}} & (\log_{10}\sigma_{\mathrm{p}})^2 \end{bmatrix}, \tag{S2}$$

where $m_{p,g,}$ and $m_{rBC,g}$ represent the geometric mean of the total particle and rBC mass, respectively; and σ_{rBC} and σ_p are the geometric standard deviation of particle and rBC mass. The covariance is parameterized using the correlation between the particle and rBC mass in logarithmic

space, R_{12}, which controls the broadness (R_{12} = 0 for very broad distributions and R_{12} = 1 for very slender distributions) of the m_p-m_{rBC} distributions. Unlike Sipkens et al., the current distributions are constrained by the fact that $m_p \geq m_{rBC}$ (Naseri et al., 2020), as the mass of rBC cannot exceed the total particle mass. The distribution is truncated accordingly.

1.2 Parameters for representative atmospheric distributions

Parameters are chosen to represent a wide range of black carbon mixing states found in the atmosphere following a condensation process and based on several studies (Gong et al., 2016; McMeeking et al., 2010; Yu et al., 2019). McMeeking et al. (2010), for example, conducted aircraft measurements of rBC aerosol concentrations in the lower troposphere over Europe using the SP2, spanning remote continental regions to highly populated urban areas. They reported a mass median diameter (MMD) and geometric standard deviation (GSD) of rBC mass of d_{MMD} = 183 nm and σ_{rBC} = 2.08, respectively. Transforming to the quantities of interest here follows from using the Hatch-Choate equation,

$$d_{\mathrm{CMD}} = d_{\mathrm{MMD}} \exp[-3(\ln \sigma_{\mathrm{rBC}})], \tag{S3}$$

to convert this mass median diameter of rBC to its equivalent count median diameter (CMD) and

$$m_{\mathrm{rBC,g}} = \rho_{\mathrm{eff}} \frac{\pi d_{\mathrm{CMD}}^3}{6} \tag{S4}$$

to convert to a median rBC mass using the same rBC density of ρ_{eff} = 1800 kg/m^3 as used by McMeeking et al. (2010). For the McMeeking et al. parameters, d_{CMD} = 135.6 nm and $m_{rBC,g}$ = 2.35 fg.

Phantoms were created which model a simple condensation process in the atmosphere, that is, the geometric mean rBC mass and geometric standard deviation of m_{rBC} were the same in all phantoms (*i.e.* the rBC particles are unchanged through the condensation process and coagulation is neglected).

As noted above, the covariance in Eq. (S2) is parameterized using a correlation, R_{12}, between two types of particle mass, thereby specifying the breadth of the m_p-m_{rBC} distribution. Specifically, we assume that high rBC mass fractions are associated with very thin or non-existent coatings and thus very narrow distributions. Conversely, particles with a substantial non-refractory component are associated with thick coatings and broad distributions. Futhermore, it was assumed that the GSD of the particle mass is equal to the GSD of the rBC mass (*i.e.*, $\sigma_p = \sigma_{rBC}$=2.08), which is an arbitrary constraint, but one that is approximately observed by Yu et al. (2020). This is implemented by stating R_{12} as a function of $m_{p,g}$,

$$R_{12} = -(3.0 \times 10^{-4}){m_{p,g}}^2 + (2.2 \times 10^{-3})m_{p,g} + 9.9 \times 10^{-1}. \quad \text{(S5)}$$

Given that $m_{rBC,g}$ = 2.35 fg is taken as a constant in the associated paper, this acts as a surrogate for the mass fraction of non-rBC in the particles for the sampling procedure described subsequently. It must be emphasized that the form of this relation is purely empirical, derived qualitatively based on observations of uncoated aerosols and the coated urban aerosols observed by Yu et al. (2020), using two-dimensional particle mass-rBC mass distributions, and studies by Liu et al. (2014) and Gong et al. (2016), which demonstrate how the aging processes affects the coating thickness of rBC-containing particles.

Throughout this work, $m_{rBC,g}$, σ_p, and σ_{rBC} are fixed at the values reported in Table A.1, while $m_{p,g}$ is sampled to realize the range of phantoms shown in. The quantity N_{tot} is sampled randomly over the range of [10, 10^6] cm^{-3} to span the range of atmospheric number concentrations from clean and heavy air pollution episodes (Chenget al., 2018; Gong et al., 2016; Wang et al., 2014; Reddington et al., 2013) and combustion sources (*e.g.*, Sipkens et al., 2021)

Table A.1. Parameters used in the generation of hypothetical two-dimensional particle mass-BC mass distributions.

$m_{rBC,g}$ [fg]	$m_{p,g}$ [fg]	σ_{rBC}	σ_p	m_p [fg]	m_{rBC} [fg]

2.35	Sampled	2.08	2.08	0.3-300	0.3-300

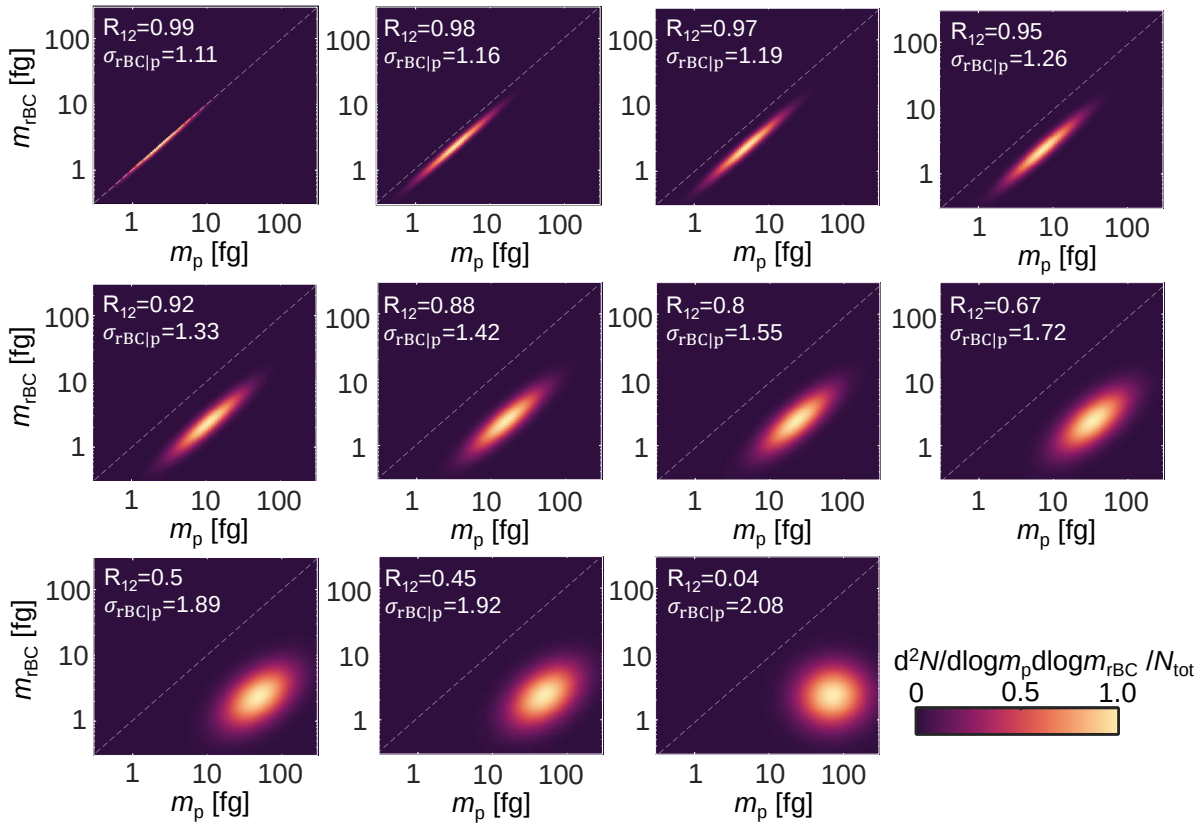

FigS. 1 Different non-dimensionalized phantoms with diverse variability of non-refractory components between particles randomly generated for synthetic data fabrication.

2 An alternative parameterization using the conditional width

Following Sipkens et al. (2020b), the above representation can also be phrased in terms of a conditional geometric standard deviation, $\sigma_{rBC|p}$. This quantity represents the width of vertical slices through the 2D distributions, as shown in FigS 2.

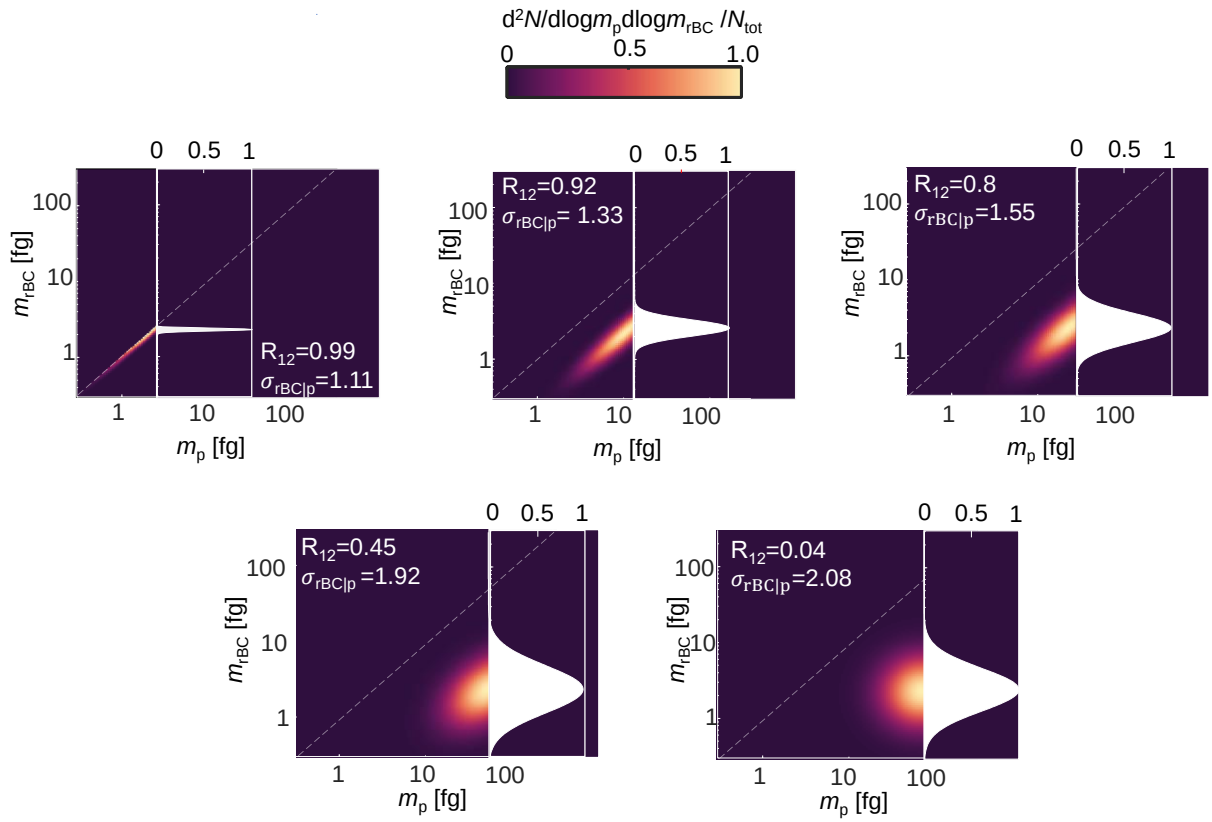

FigS. 2 . Different non-dimensionalized phantoms with the conditional distributions.

For very narrow distributions, where $R_{12} = 1$, $\sigma_{\mathrm{rBC|p}} = 1$; for wide distributions, where $R_{12} = 0$, $\sigma_{\mathrm{rBC|p}} = \sigma_{\mathrm{rBC}}$. As such, this parameter can replace R_{12} in the definition of the bivariate lognormal distribution to give,

$$p(m_{\mathrm{p}}, m_{\mathrm{rBC}}) = \frac{N_{\mathrm{tot}}}{2\pi m_{\mathrm{p}} m_{\mathrm{rBC}} \ln\sigma_{\mathrm{p}} \ln\sigma_{\mathrm{rBC|p}}} \exp\left\{-\frac{1}{2}\left(\frac{\ln m_{\mathrm{p}} - \ln m_{\mathrm{p,g}}}{\ln\sigma_{\mathrm{p}}}\right)^2 - \frac{1}{2}\left(\frac{\ln m_{\mathrm{rBC}} - \ln(m_{\mathrm{rBC,g}}|m_{\mathrm{p}})}{\ln\sigma_{\mathrm{rBC|p}}}\right)^2\right\}, \tag{S6}$$

where $m_{\mathrm{rBC,g}}|m_{\mathrm{p}}$ is the conditional geometric mean rBC mass, and $\sigma_{\mathrm{rBC|p}}$ is the conditional geometric standard deviation, which be derived from $\mathbf{\Sigma}$ in Eq. (S4) using (Bertsekas & Tsitsiklis, 2002),

$$\log_{10}\sigma_{rBC|p} = \sqrt{\Sigma_{1,1}(1 - R_{1,2}^2)}. \quad \text{(S7)}$$

FigS 3. shows this relationship, where the condition geometric standard deviation changes from $\sigma_{rBC|p} = 1.0$ when $R_{12} = 1$ to $\sigma_{rBC|p} = \sigma_{rBC}$ when $R_{12} = 0$.

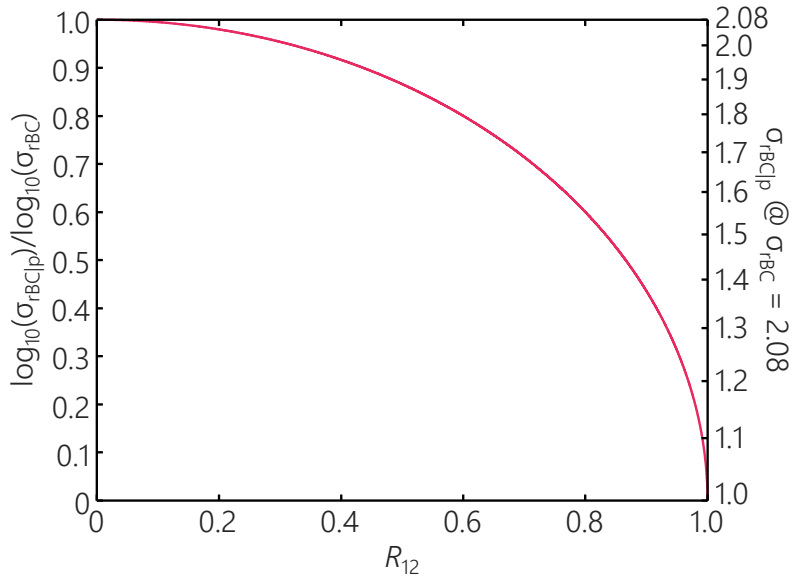

FigS. 3 . Relationship between the correlation, R_{12}, and the conditional distribution geometric standard deviation, $\boldsymbol{\sigma}_{rBC|p}$.

3 Trends in optimum Tikhonov regularization parameter with the distribution width

FigS. 4 indicates a positive correlation between the optimal Tikhonov regularization parameter and the width of the distribution. While larger regularization parameters are often associated with lower errors, these large regularization parameters are only reasonable for broad phantoms. Generally, broader distributions respond better to prior information (via the Tikhonov

regularization scheme) that encodes smoothness. By contrast, very narrow phantoms will have their edges smoothed away by the prior, requiring lower regularization parameters to preserve sharpness. At the same time, the smaller regularization parameter will increase the amount of noise that propagates forward into the reconstructions, such that the minimum achievable error is larger. Some of this may be overcome using a different prior, e.g., exponential distance prior (Naseri et al., 2020; Sipkens et al., 2020b) or a total variation prior.

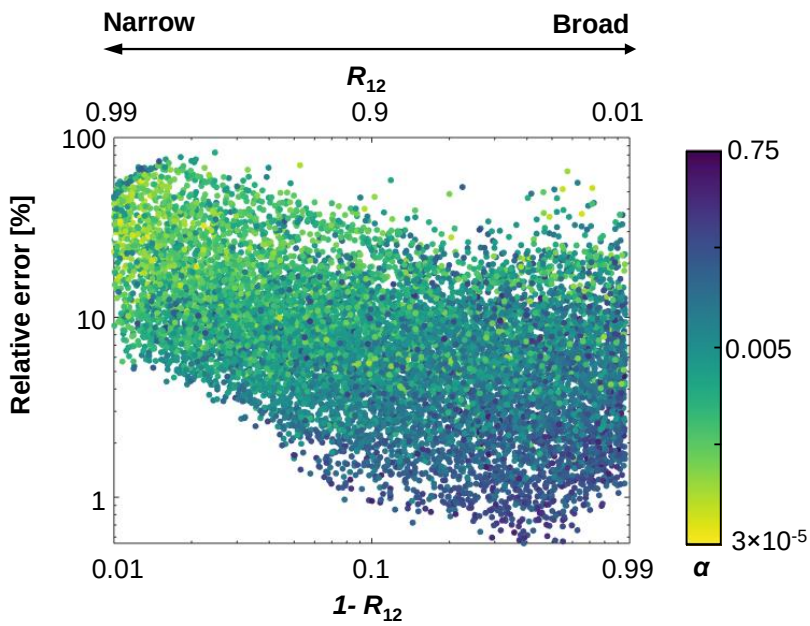

FigS. 4. The sensitivity of reconstruction accuracy to R_{12} indices (i.e., distributions' broadness) and colored with the regularization parameter.

4 References

Bertsekas, D. P., & Tsitsiklis, J. N. (2002). The bivariate normal distribution. *Introduction to Probability*, 247–253.

Broda, K. N., Olfert, J. S., Irwin, M., Schill, G. P., McMeeking, G. R., Schnitzler, E. G., & Jäger, W. (2018). A novel inversion method to determine the mass distribution of non-refractory coatings on refractory black carbon using a centrifugal particle mass analyzer and single particle soot photometer. *Aerosol Science and Technology*, *52*(5), 567–578. https://doi.org/10.1080/02786826.2018.1433812

Cheng, Y., Li, S.-M., Gordon, M., & Liu, P. (2018). Size distribution and coating thickness of black carbon from the Canadian oil sands operations. *Atmospheric Chemistry and Physics*, *18*(4), 2653–2667.

Gong, X., Zhang, C., Chen, H., Nizkorodov, S. A., Chen, J., & Yang, X. (2016). Size distribution and mixing state of black carbon particles during a heavy air pollution episode in Shanghai. *Atmospheric Chemistry and Physics*, *16*(8), 5399–5411.

Liu, D., Allan, J. D., Young, D. E., Coe, H., Beddows, D., Fleming, Z. L., … Lee, J. (2014). Size distribution, mixing state and source apportionment of black carbon aerosol in London during wintertime. *Atmospheric Chemistry and Physics*, *14*(18), 10061–10084.

McMeeking, G. R., Hamburger, T., Liu, D., Flynn, M., Morgan, W. T., Northway, M., … Coe, H. (2010). Black carbon measurements in the boundary layer over western and northern Europe. *Atmospheric Chemistry and Physics*, *10*(19), 9393–9414. https://doi.org/10.5194/acp-10-9393-2010

Naseri, A., Sipkens, T. A., Rogak, S. N., & Olfert, J. S. (2020). An improved inversion method for determining two-dimensional mass distributions of non-refractory materials on refractory black carbon. *Aerosol Science and Technology*, (just-accepted), 1–17.

Reddington, C. L., McMeeking, G., Mann, G. W., Coe, H., Frontoso, M. G., Liu, D., … Carslaw, K. S. (2013). The mass and number size distributions of black carbon aerosol over Europe. *Atmospheric Chemistry and Physics*, *13*(9), 4917–4939.

Sipkens, T. A., Olfert, J. S., & Rogak, S. N. (2020). Inversion methods to determine two-dimensional aerosol mass-mobility distributions II: Existing and novel Bayesian methods. *Journal of Aerosol Science*, *146*, 105565. https://doi.org/10.1016/j.jaerosci.2020.105565

Sipkens, Timothy A., Trivanovic, U., Naseri, A., Bello, O. W., Baldelli, A., Kazemimanesh, M., … Rogak, S. N. (2021). Using two-dimensional distributions to inform the mixing state of soot and salt particles produced in gas flares. *Journal of Aerosol Science*, *158*, 105826. https://doi.org/10.1016/j.jaerosci.2021.105826

Wang, Q., Schwarz, J. P., Cao, J., Gao, R., Fahey, D. W., Hu, T., … Shen, Z. (2014). Black carbon aerosol characterization in a remote area of Qinghai–Tibetan Plateau, western China. *Science of the Total Environment*, *479*, 151–158.

Yu, C., Liu, D., Broda, K., Joshi, R., Olfert, J., Sun, Y., … Allan, J. D. (2019). Characterising Mass-resolved Mixing State of Black Carbon in Beijing Using a Morphology-Independent Measurement Method. *Geophysical Research Abstracts*, *21*.

Yu, C., Liu, D., Broda, K., Joshi, R., Olfert, J., Sun, Y., … D. Allan, J. (2020). Characterising mass-resolved mixing state of black carbon in Beijing using a morphology-independent measurement method. *Atmospheric Chemistry and Physics*, *20*(6), 3645–3661. https://doi.org/10.5194/acp-20-3645-2020